Phase estimation via number-conserving operation inside the SU(1,1) interferometer

Qingqian Kang[1,2], Zekun Zhao[1], Teng Zhao[1], Cunjin Liu[1], and Liyun Hu[1,3*]

[1]*Center for Quantum Science and Technology, Jiangxi Normal University, Nanchang 330022, China*
[2]*Department of Physics, Jiangxi Normal University Science and Technology College, Nanchang 330022, China*
[3]*Institute for Military-Civilian Integration of Jiangxi Province, Nanchang 330200, China*

Utilizing nonlinear elements, SU(1,1) interferometers demonstrate superior phase sensitivity compared to passive interferometers. However, the precision is significantly impacted by photon losses, particularly internal losses. We propose a theoretical scheme to improve the precision of phase measurement using homodyne detection by implementing number-conserving operation (NCO), i.e., $aa^\dagger$ and $a^\dagger a$, inside the SU(1,1) interferometer, with the coherent state and the vacuum state as the input states. We analyze the effects of NCO on the phase sensitivity, the quantum Fisher information (QFI), and the quantum Cramér-Rao bound (QCRB) under both ideal and photon losses scenarios. Our findings reveal that the internal non-Gaussian operations can enhance the phase sensitivity and the QFI, and effectively improve the robustness of the SU(1,1) interferometer against internal photon losses. Notably, the $a^\dagger a$ scheme exhibits superior improvement in both ideal and photon losses cases in terms of phase sensitivity. Moreover, in the ideal case, $aa^\dagger$ scheme slightly outperforms $a^\dagger a$ scheme in terms of the QFI. However, in the presence of high photon losses, $a^\dagger a$ scheme demonstrates a greater advantage.

PACS: 03.67.-a, 05.30.-d, 42.50,Dv, 03.65.Wj

I. INTRODUCTION

Optical interference measurement plays a crucial role in many scientific and technological applications such as quantum metrology for precise measurements, imaging for capturing detailed visual information, sensing for detecting and measuring physical quantities, and information processing for manipulating and transmitting data [1–9]. Consequently, there has been extensive research and significant advancements in the field of optical interference measurement. To satisfy the need for high precision, a variety of optical interferometers have been proposed and developed. One of the most practical interferometers is the Mach-Zehnder interferometer (MZI), whose phase sensitivity is limited by the standard quantum-noise limit (SQL) $\Delta\phi = 1/\sqrt{N}$ (N is the average number of photons within the interferometer), together with solely classical resources as the input of the MZI [10]. Over recent decades, various schemes have been proposed to improve the phase sensitivity of the traditional MZI [11, 12]. It has been demonstrated that the quantum states as the input states to make the traditional MZI beat the SQL. For example, NOON state [13, 14], twin Fock state [15], and the squeezed state [16, 17] *et al.* can achieve or even exceed the Heisenberg limit (HL) $\Delta\phi = 1/N$ [18, 19].

Another possibility to realize quantum-enhanced phase sensitivity is the SU(1,1) interferometer [20, 21], which replaced traditional linear beam splitters (BSs) with optical parametric amplifiers (OPAs). It splits and mixes beams using nonlinear transformations, which is first proposed by Yurke *et al.* [22]. In the SU(1,1) interferometer comprising two OPAs, the first OPA serves

the dual purpose of acquiring entangled resources and suppressing amplified noise. Meanwhile, the subsequent use of the second OPA can lead to signal enhancement, offering a viable pathway for achieving higher precision in phase estimation. By utilizing entangled photon states, the SU(1,1) interferometer can surpass the SQL, enabling higher precision. This technique revolutionized phase estimation, becoming a vital tool in quantum precision measurements. Then, there has been significant interest in studying the SU(1,1) interferometer [23–25]. For instance, Hudelist *et al.* demonstrated that the gain effect of OPA results in the SU(1,1) interferometer exhibiting higher sensitivity compared to traditional linear interferometers [27]. In 2011, Jing *et al.* [28] successfully implemented this interferometer experimentally. In this nonlinear interferometer, the maximum output intensity can be much higher than that of linear interferometer due to the OPA. Apart from the standard form, various configurations of SU(1,1) interferometer have also been proposed [24, 29–37].

As previously mentioned, although SU(1,1) interferometer is highly valuable for precision measurement [38, 39], the precision is still affected by dissipation, particularly photon losses inside the interferometer [40, 41]. Consequently, to further enhance precision, non-Gaussian operations should serve as an effective approach to mitigate internal dissipation. Most theoretical [42–45] and experimental [46–48] studies have fortunately indicated that non-Gaussian operations, such as photon subtraction (PS), photon addition (PA), photon catalysis (PC), quantum scissor and their coherent superposition, are effectively enhancing the nonclassicality and entanglement degrees of quantum states, thereby enhancing their potential in quantum information processing [49, 50]. Experimental studies have illustrated the conditional generation of superpositions of distinct quantum operations through single-photon in-

terference, providing a practical approach for preparing non-Gaussian operations [51]. This advancement has unveiled new possibilities in quantum state manipulation and implications for various quantum technologies. In Ref. [52], Zhang et al. proposed a number-conserving operation (NCO) on the inputs of MZI for improving the resolution and precision of phase measurement with parity detection. It is shown that the phase sensitivity can be better than that of both the photon subtraction operation and photon addition operation, in the presence of photon losses. Different from Ref. [52], Xu et al. examined the phase sensitivity with internal photon losses in SU(1,1) interferometers, rather than in the MZI, an SU(2) interferometer. It is found that performing photon addition operations internally provides superior results compared to those at the input [53]. Thus, a question arises naturally: can the NCO be operated inside the SU(1,1) interferometer (i.e., the non-Gaussian operation on the output states after first OPA) to mitigate the impact of internal photon losses?

Therefore, in this paper, we concentrate on employing the NCO scheme inside the SU(1,1) interferometer to enhance the measurement accuracy , and then analyze the improvement effect of internal non-Gaussian operation on the phase sensitivity and the QFI in the presence of photon losses. The remainder of this paper is arranged as follows. Sec. II outlines the theoretical model of the NCO. Sec. III delves into phase sensitivity, encompassing both ideal and internal photon losses cases. Sec. IV centers on the QFI and QCRB [54, 55]. Finally, Sec. V provides a comprehensive summary.

II. MODEL

This section begins with an introduction to the SU(1,1) interferometer, as illustrated in Fig. 1(a). The SU(1,1) interferometer typically consists of two OPAs and a linear phase shifter, making it one of the most commonly used interferometers in quantum metrology research. The first OPA is characterized by a two-mode squeezing operator $U_{S_1}(\xi_1) = \exp(\xi_1^* ab - \xi_1 a^\dagger b^\dagger)$, where a and b, $a^\dagger$ and $b^\dagger$ represent the photon annihilation and creation operators, respectively. The squeezing parameter ξ_1 can be expressed as $\xi_1 = g_1 e^{i\theta_1}$, where g_1 represents the gain factor and θ_1 represents the phase shift. This parameter plays a critical role in shaping the interference pattern and determining the system's phase sensitivity. Following the first OPA, mode a undergoes a phase shift process $U_\phi = \exp[i\phi(a^\dagger a)]$, while mode b remains unchanged. Subsequently, the two beams are coupled in the second OPA with the operator $U_{S_2}(\xi_2) = \exp(\xi_2^* ab - \xi_2 a^\dagger b^\dagger)$, where $\xi_2 = g_2 e^{i\theta_2}$ and $\theta_2 - \theta_1 = \pi$. In this paper, we set the parameters $g_1 = g_2 = g$, $\theta_1 = 0$, $\theta_2 = \pi$. We utilize the coherent state $|\alpha\rangle_a$ and the vacuum state $|0\rangle_b$ as input states and homodyne detection is employed on the mode a of the output.

The SU(1,1) interferometer is generally susceptible

to photon losses, particularly in the case of internal losses. To simulate photon losses, the use of fictitious BSs is proposed, as depicted in Fig. 1(a). The operators of these fictitious BSs can be represented as $U_B = U_{B_a} \otimes U_{B_b}$, with $U_{B_a} = \exp\left[\theta_a\left(a^\dagger a_v - a a_v^\dagger\right)\right]$ and $U_{B_b} = \exp\left[\theta_b\left(b^\dagger b_v - b b_v^\dagger\right)\right]$, where a_v and b_v represent vacuum modes. Here, T_k ($k = a, b$) denotes the transmissivity of the fictitious BSs, associated with θ_k through $T_k = \cos^2 \theta_k \in [0, 1]$. The value of transmittance equal to 1 ($T_k = 1$) corresponds to the ideal case without photon losses [53]. In an expanded space, the expression for the output state of the standard SU(1,1) interferometer can be represented as the following pure state, i.e.,

$$\left|\Psi_{out}^0\right\rangle = U_{S_2} U_\phi U_B U_{S_1} |\psi_{in}\rangle, \tag{1}$$

where $|\psi_{in}\rangle = |\alpha\rangle_a |0\rangle_b |0\rangle_{a_v} |0\rangle_{b_v}$.
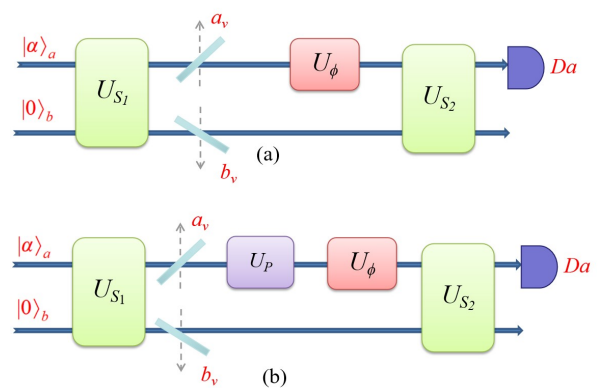

FIG. 1. Schematic diagram of the SU(1,1) interferometer. (a) the standard SU(1,1) interferometer, (b) the SU(1,1) interferometer with NCO. The two input ports are a coherent state $|\alpha\rangle_a$ and a vacuum state $|0\rangle_b$. a_v and b_v are vacuum modes. U_{S_1} and U_{S_2} are the optical parametric amplifiers, U_ϕ is the phase shifter. U_P is the NCO operator and D_a is the homodyne detector.

To mitigate the impact of photon losses, we introduce a distinct non-Gaussian operation inside the SU(1,1) interferometer, called the NCO scheme, as illustrated in Fig. 1(b). We utilize simple and easy-to-prepare input states ($|\alpha\rangle_a \otimes |0\rangle_b$), and an experimentally feasible homodyne detection. As referred to Ref. [45], the NCO can be seen as an equivalent operator, i.e.,

$$U_P = s a a^\dagger + t a^\dagger a, \tag{2}$$

where $s^2 + t^2 = 1$ with s and t being real numbers, a and $a^\dagger$ are annihilation operator and creation operator, respectively. From Eq. (2), one can obtain the photon addition then photon subtraction (PA-then-PS) $a a^\dagger$, and photon subtraction then photon addition (PS-then-PA) $a^\dagger a$, respectively. The process can be described by operator U_{P_j}, where $j = 1$ and 2, $U_{P_1} = a a^\dagger$ and $U_{P_2} = a^\dagger a$, respectively. Actually, the NCOs $a a^\dagger$ and $a^\dagger a$ are non-Gaussian operations, which can be experimentally realized via conditional measurement, like a and $a^\dagger$. For instance, on the basis of BS with high transmissivity and a

photon detection, one can arrive at the experimental implementation of a single PS [48]. In addition, PA operation can be implemented by four-wave mixing technique, and it is also implemented by BS with zero photon detection and single photon input [56, 57]. When the two consecutive conditional measurements are achieved, the quantum state corresponding to the detected results is selected to be our study object. In the ideal case, the obtained state is not a mixed state but a pure one for a pure input.

In this case of NCO applying inside the SU(1,1) interferometer, the output state can be written as the following pure states

$$\left| \Psi_{out}^1 \right\rangle = A_1 U_{S_2} U_\phi U_{p_1} U_B U_{S_1} \left| \psi_{in} \right\rangle, \tag{3}$$

and

$$\left| \Psi_{out}^2 \right\rangle = A_2 U_{S_2} U_\phi U_{p_2} U_B U_{S_1} \left| \psi_{in} \right\rangle. \tag{4}$$

A_1 and A_2 are the normalization constants for the PA-then-PS and PS-then-PA, respectively, given by [53]

$$A_1 = \left(P_{2,2,0,0} + 3P_{1,1,0,0} + 1 \right)^{-\frac{1}{2}}, \tag{5}$$

$$A_2 = \left(P_{2,2,0,0} + P_{1,1,0,0} \right)^{-\frac{1}{2}}, \tag{6}$$

where $P_{x_1,y_1,x_2,y_2} = \partial^{x_1+y_1+x_2+y_2}/\partial\lambda_1^{x_1}\partial\lambda_2^{y_1}\partial\lambda_3^{x_2}\partial\lambda_4^{y_2}$ $\{e^{w_4}\}|_{\lambda_1=\lambda_2=\lambda_3=\lambda_4=0}$, as well as

$$w_1 = \lambda_1 T \left(\lambda_2 \sinh g - \lambda_3 \cosh g \right) \sinh g$$
$$\quad + \lambda_4 T \left(\lambda_3 \sinh g - \lambda_2 \cosh g \right) \sinh g, \tag{7}$$

$$w_2 = \lambda_1 \sqrt{T} \cosh g - \lambda_4 \sqrt{T} \sinh g, \tag{8}$$

$$w_3 = \lambda_2 \sqrt{T} \cosh g - \lambda_3 \sqrt{T} \sinh g, \tag{9}$$

$$w_4 = w_1 + w_2 \alpha^* + w_3 \alpha. \tag{10}$$

III. PHASE SENSITIVITY

Quantum metrology is an effective approach utilizing quantum resources for precise phase measurements [58, 59]. The objective is to achieve highly sensitive measurements of unknown phases. Within this section, we delve further into investigating the phase sensitivity for the NCO inside the SU(1,1) interferometer [60]. Various detection methods are available for this purpose, such as homodyne detection [61, 62], parity detection [16, 63], and intensity detection [64]. Each of these methods offers different trade-offs between sensitivity, complexity, and practical implementation. It is important to note that the phase sensitivities of different detection schemes may vary for different input states and interferometers [65]. Each measurement method has its own advantages. In many schemes, parity detection has been proven to be the optimal detection method for linear phase estimation [16, 19], but it is relatively complex and is harder to implement experimentally. In Ref. [61], it is noted that the phase sensitivity of an SU(1,1) interferometer

with homodyne detection surpasses that with intensity detection. Homodyne detection is not only easy to implement with current experimental technology [56], but also simple from a theoretical calculation perspective, thereby playing a key role in the field of continuous-variable quantum key distribution [66, 67]. For this reason, we use the homodyne detection on mode a at one output port to estimate the phase sensitivity.

In homodyne detection, the measured variable is one of the two orthogonal components of the mode a, given by $X = (a + a^\dagger)/\sqrt{2}$. Based on the error propagation equation [22], the phase sensitivity can be expressed as

$$\Delta\phi = \frac{\sqrt{\langle \Delta^2 X \rangle}}{\left| \partial \langle X \rangle / \partial\phi \right|} = \frac{\sqrt{\langle X^2 \rangle - \langle X \rangle^2}}{\left| \partial \langle X \rangle / \partial\phi \right|}. \tag{11}$$

Based on Eqs. (3), (4) and (11), the phase sensitivity for the NCO can be theoretically determined. The detail calculation steps for the phase sensitivity $\Delta\phi$ of the PA-then-PS and PS-then-PA are provided in Appendix A.

A. Ideal case

Initially, we consider the ideal case, $T_k = 1$ (where $k = a, b$), representing the scenario without photon losses. The phase sensitivity $\Delta\phi$ is plotted as a function of ϕ in Fig. 2. Fig. 2(a) is for different superposition operations, from which it is observed that when $0 < t < 1$ (dashed line), the phase sensitivity consistently falls between the extremes of $t = 0$ (red solid line) and $t = 1$ (blue solid line), which correspond to PA-then-PS and PS-then-PA, respectively. This indicates that the effects of superposition operations are between PS-then-PA and PA-then-PS on the improvement of phase sensitivity. Thus, for the sake of simplicity, our subsequent investigation concentrates only on these two boundary cases. Fig. 2(b) is for the standard and these two boundary cases. It is shown that (i) The phase sensitivity improves initially and then decreases as the phase increases, with the optimal sensitivity deviating from $\phi = 0$. (ii) Both PA-then-PS and PS-then-PA effectively enhance the phase sensitivity $\Delta\phi$. (iii) The phase sensitivity of PS-then-PA is better than that of PA-then-PS, and the difference increases with increasing phase.

Fig. 3 illustrates that the phase sensitivity $\Delta\phi$ plotted against the gain factor g for different schemes. The plot confirms that an increase in the gain factor g enhances the phase sensitivity. It is interesting to notice that, when the g value is small, the PA-then-PS demonstrates a better improvement. Conversely, when the g value is large, the opposite is true. Although the improvement of both is related to parameter g, the PS-then-PA is better in terms of accuracy, i.e., the PS-then-PA achieves the optimal phase sensitivity. Thus, the following studies mainly focus on the large parameter g.

Similarly, we analyze the phase sensitivity $\Delta\phi$ as a function of the coherent amplitude α, as depicted in
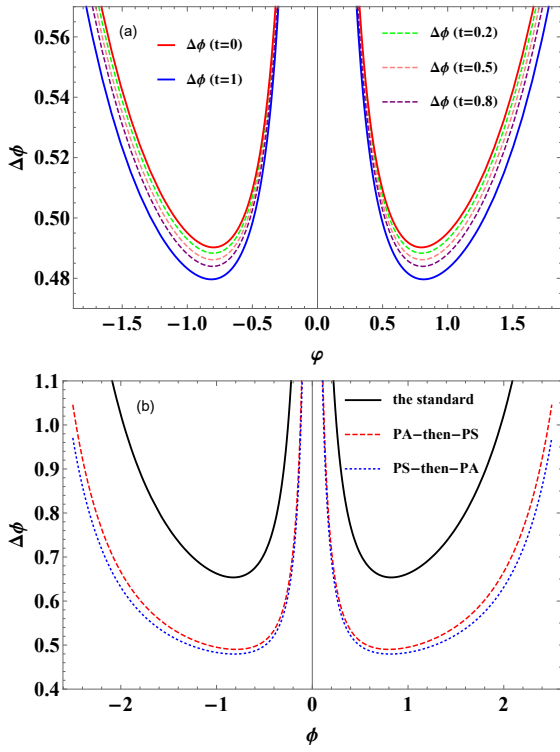
FIG. 2. The phase sensitivity of NCO based on the homodyne detection as a function of ϕ with $\alpha = 1$ and $g = 1$. (a) The phase sensitivity for different values of the parameter t. (b) The black solid line corresponds to the standard SU(1,1) interferometer; the red dashed line and the blue dotted line correspond to the PA-then-PS and PS-then-PA, respectively.
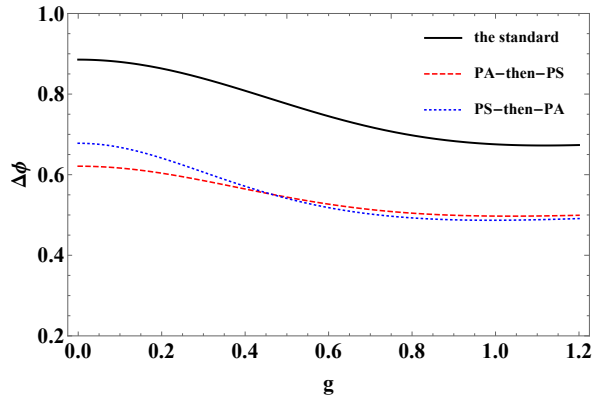

FIG. 3. The phase sensitivity as a function of g, with $\alpha = 1$ and $\phi = 0.6$.

Fig. 4. The phase sensitivity improves with the coherent amplitude α, attributed to the increase in the mean photon number with α, then enhancing intramode correlations and quantum entanglement between the two modes. Furthermore, the enhancement effect diminishes as the coherent amplitude α increases. It is noteworthy that the PS-then-PA demonstrates better improvement than the PA-then-PS at small values of α, while the

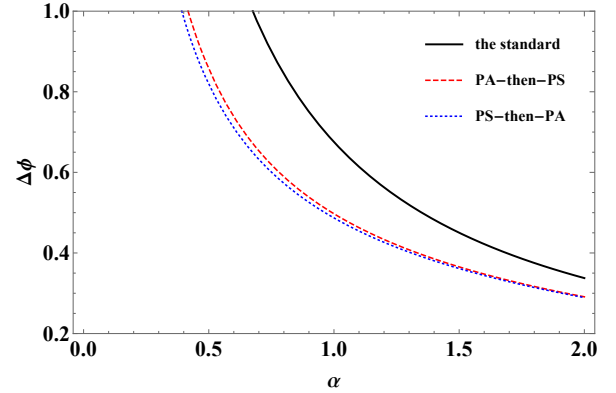improvement effects of both schemes are consistent at larger values of α.

FIG. 4. The phase sensitivity as a function of α, with $g = 1$ and $\phi = 0.6$.

B. Photon losses case

The SU(1,1) interferometer plays a critical role in achieving high-precision measurements. However, precision is significantly affected by photon losses, particularly internal losses. Here, we focus on internal photon losses, corresponding to $T_k \in (0, 1)$. The phase sensitivity, depicted as a function of transmittance T_k in Fig. 5 for fixed g, α, and ϕ, improves as anticipated with higher transmittance T_k. Lower transmittance corresponds to increased internal losses, weakening the performance of phase estimation. Both PA-then-PS and PS-then-PA schemes within the SU(1,1) interferometer effectively enhance the phase sensitivity $\Delta\phi$. Moreover, it is notable that as transmittance T_k increases, the improvement in phase sensitivity first increases and then decreases for both schemes. Notably, the PS-then-PA scheme consistently demonstrates higher phase sensitivity than the PA-then-PA scheme across the entire range.
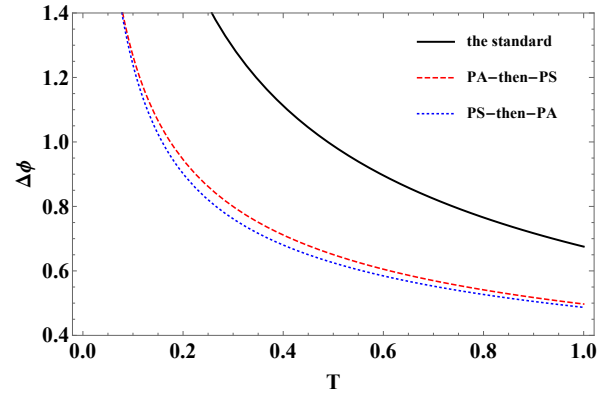

FIG. 5. The phase sensitivity as a function of transmittance T_k, with $g = 1$, $\phi = 0.6$ and $\alpha = 1$.

The robustness to photon losses denotes the measurement process's insensitivity to photon losses. A quantum precision measurement system with strong robustness can maintain high accuracy and stability even in the presence of photon losses, thereby reducing measurement errors and uncertainties. By designing and optimizing interferometer measurement processes, the system's robustness to photon losses can be improved.

To better study the enhancing effect of the NCO on robustness against photon losses, we further compare the changes of the phase sensitivity in ideal and photon losses cases for different schemes, as shown in Fig. 6. The comparison reveals that the phase sensitivity of the standard SU(1,1) interferometer is more significantly affected by photon losses. In contrast, the phase sensitivity of the NCO is less affected, indicating that the non-Gaussian operations can mitigate the impact of internal photon losses and enhance the interferometer's robustness against losses.
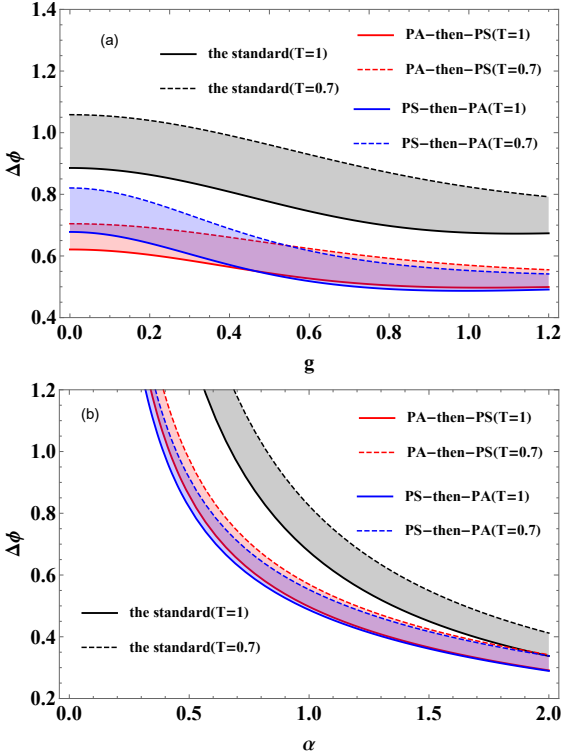

FIG. 6. The comparisons for robustness against photon losses. (a) The phase sensitivity as a function of g, with $\alpha = 1$ and $\phi = 0.6$. (b) The phase sensitivity as a function of α, with $g = 1$ and $\phi = 0.6$.

C. Comparison with SQL and HL

Additionally, we compare the phase sensitivity with SQL and HL in this subsection. The SQL and HL are defined as $\Delta\phi_{SQL} = 1/\sqrt{N_j}$ and $\Delta\phi_{HL} = 1/N_j$, respec-

tively. Here N_j represents the total mean photon number inside the interferometer before the second OPA for each scheme [68, 69], $j = 1$ or 2. N_j can be calculated as

$$
\begin{aligned}
N_1 &= A_1^2 \langle\psi_{in}|U_{S_1}^\dagger U_B^\dagger U_{P_1}^\dagger \left(a^\dagger a + b^\dagger b\right) U_{P_1} U_B U_{S_1}|\psi_{in}\rangle \\
&= A_1^2 (P_{3,3,0,0} + 5P_{2,2,0,0} + 4P_{1,1,0,0} \\
&\quad + P_{2,2,1,1} + 3P_{1,1,1,1} + P_{0,0,1,1}),
\end{aligned} \tag{12}
$$

for the PA-then-PS and

$$
\begin{aligned}
N_2 &= A_2^2 \langle\psi_{in}|U_{S_1}^\dagger U_B^\dagger U_{P_2}^\dagger \left(a^\dagger a + b^\dagger b\right) U_{P_2} U_B U_{S_1}|\psi_{in}\rangle \\
&= A_2^2 (P_{3,3,0,0} + 3P_{2,2,0,0} + P_{1,1,0,0} \\
&\quad + P_{2,2,1,1} + P_{1,1,1,1}),
\end{aligned} \tag{13}
$$

for the PS-then-PA, respectively.

For these two schemes at fixed g and α, we plot the phase sensitivity $\Delta\phi$ as a function of ϕ for a comparison with the SQL and the HL of the standard SU(1,1) interferometer. Our findings demonstrate that (i) the original interferometer (without NCO) cannot surpass the SQL. (ii) The NCO schemes are capable of surpassing the SQL within a wide range, even in the presence of significant photon losses (Fig. 7(b)). This suggests that the NCO schemes show better robustness against internal photon losses. (iii) The phase sensitivity of PS-then-PA is better than that of PA-then-PS.
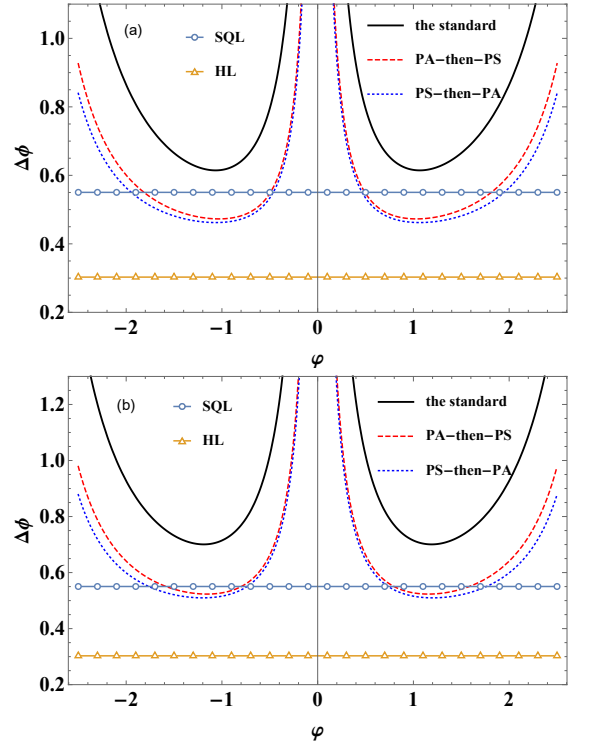

FIG. 7. Comparison of phase sensitivity with the SQL and HL for fixed $g = 0.7$ and $\alpha = 1$. The blue circle is the SQL and the yellow triangle is the HL. (a) $T = 1$, (b) $T = 0.7$.

IV. THE QUANTUM FISHER INFORMATION

In the previous discussions, we have explored the influence of NCO schemes on phase sensitivity and the correlation between phase sensitivity and relevant parameters using homodyne detection. It is crucial to recognize that the discussed phase sensitivity is influenced by the chosen measurement method. Hence, the question arises: how can we achieve maximum phase sensitivity in an interferometer that is independent of the measurement method used? This section shifts our focus to the QFI, which represents the maximum information extracted from the interferometer system, regardless of the measurement method employed. We will examine the QFI in ideal and realistic scenarios, respectively.

A. Ideal case

For a pure state system, the QFI can be derived by [71]

$$F_j = 4\left[\langle\Psi'_j|\Psi'_j\rangle - |\langle\Psi'_j|\Psi_j\rangle|^2\right], \tag{14}$$

where $|\Psi_j\rangle$ is the quantum state after phase shift and before the second OPA, and $|\Psi'_j\rangle = \partial|\Psi_j\rangle/\partial\phi$. Then the QFI can be reformed as [71]

$$F_j = 4\langle\Delta^2 n_a\rangle, \tag{15}$$

where $\langle\Delta^2 n_a\rangle = \langle\Psi_j|(a^\dagger a)^2|\Psi_j\rangle - (\langle\Psi_j|a^\dagger a|\Psi_j\rangle)^2$.

In the ideal NCO, the quantum state is given by $|\Psi_j\rangle = A_j U_\phi U_{p_j} U_{S_1}|\alpha\rangle_a|0\rangle_b$, with $U_{P_1} = aa^\dagger$ ($j = 1$), $U_{P_2} = a^\dagger a$ ($j = 2$). Thus, the QFI is derived as

$$\begin{aligned}F_1 =\ & 4\{A_1^2\left(P_{4,4,0,0} + 8P_{3,3,0,0} + 14P_{2,2,0,0} + 4P_{1,1,0,0}\right)\\ & - \left[A_1^2\left(P_{3,3,0,0} + 5P_{2,2,0,0} + 4P_{1,1,0,0}\right)\right]^2\},\end{aligned} \tag{16}$$

for the PA-then-PS and

$$\begin{aligned}F_2 =\ & 4\{A_2^2\left(P_{4,4,0,0} + 6P_{3,3,0,0} + 7P_{2,2,0,0} + P_{1,1,0,0}\right)\\ & - \left[A_2^2\left(P_{3,3,0,0} + 3P_{2,2,0,0} + P_{1,1,0,0}\right)\right]^2\},\end{aligned} \tag{17}$$

for the PS-then-PA, respectively. In the above equations, $T_k = 1$. It is possible to explore the connection between the QFI and the related parameters using Eqs. (16) and (17).

Fig. 8 illustrates the QFI as a function of g (α) for a specific α (g). It is evident that a higher value of g (α) corresponds to a greater QFI. Both PA-then-PS and PS-then-PA result in an enhanced QFI due to the non-Gaussian nature. The QFI of PA-then-PS is slightly higher than that of PS-then-PA in both figures. Moreover, we observe that the improvement of QFI due to non-Gaussian operations increases with the increase of the value g (as shown in Fig. 8(a)), while it does not significantly change with the variation of the value α (as shown in Fig. 8(b)).
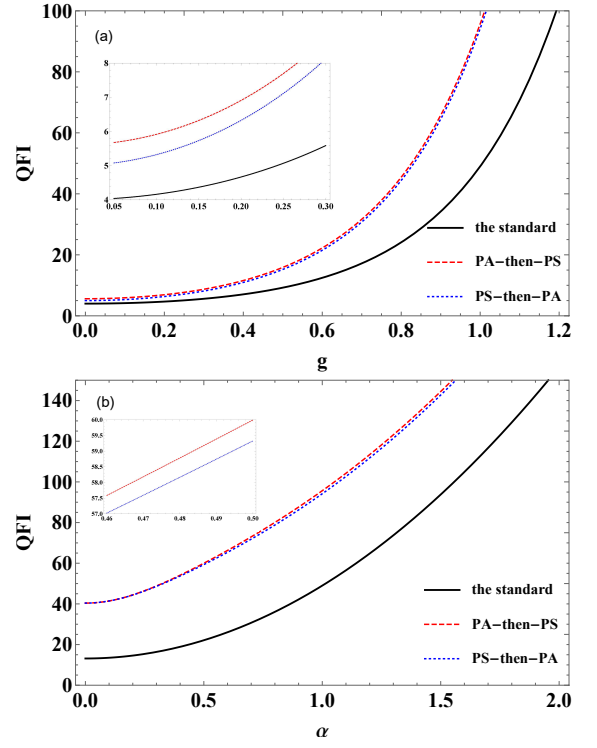

FIG. 8. (a) The QFI as a function of g, with $\alpha = 1$. (b) The QFI as a function of α, with $g = 1$.

Actually, the QFI can be associated with the phase sensitivity through [70]

$$\Delta\phi_{QCRB} = \frac{1}{\sqrt{vF}}, \tag{18}$$

where v represents the number of measurements. For simplicity, we set $v = 1$. Another quantum limit, the QCRB [54, 55], denoted as $\Delta\phi_{QCRB}$, defines the ultimate limit for a set of probabilities derived from measurements on a quantum system. It is an estimator implemented asymptotically by a maximum likelihood estimator and provides a detection-independent phase sensitivity. In order to better help us understand how optimal the phase sensitivity obtained from the SU(1,1) interferometer with the NCO really is, we compare the phase sensitivity $\Delta\phi$ obtained by using the second OPA and homodyne detection with the sensitivity $\Delta\phi_{QCRB}$ obtained from the QFI. Fig. 9 illustrates the variation of $\Delta\phi_{QCRB}$ as a function of g (α) for a specific α (g). It is shown that $\Delta\phi_{QCRB}$ improves with increasing g and α. Similarly, due to the non-Gaussian nature, both PA-then-PS and PS-then-PA are able to improve $\Delta\phi_{QCRB}$. Furthermore, the improvement in $\Delta\phi_{QCRB}$ is more obvious for small coherent amplitude α (refer to Fig. 9(b)). It is shown that for a smaller gain factor or a greater coherent amplitude, the measurement-based sensitivity better reflects Fisher information situation (described via $\Delta\phi_{QCRB}$).
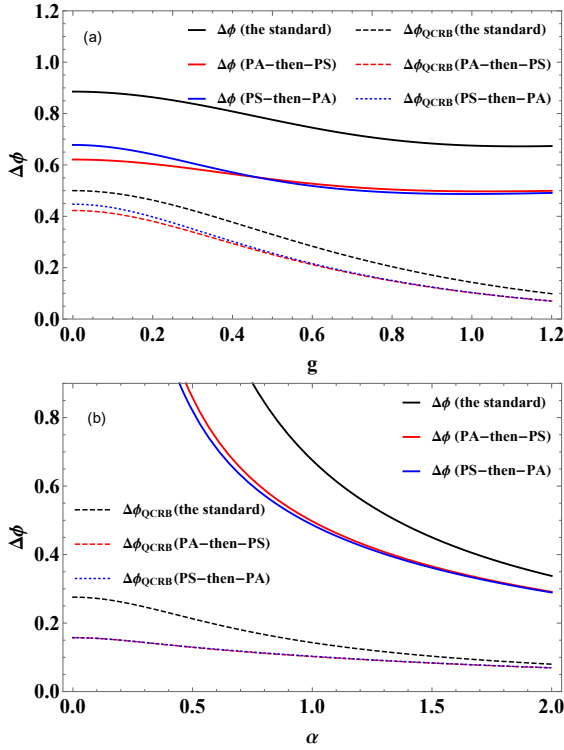
FIG. 9. Comparisons of the phase sensitivity $\Delta\phi$ obtained by homodyne detection with the ultimate sensitivity $\Delta\phi_{QCRB}$ obtained from QFI.

B. Photon losses case

In this subsection, we extend our analysis to cover the QFI in the presence of photon losses. Specifically, we examine homodyne detection on mode a, which is susceptible to photon losses. Consequently, our attention is directed toward the QFI of the system with photon losses in mode a, as depicted in Fig. 10. Here, we should emphasize that the Fisher information is obtained using the state preceding the second OPA, i.e., despite Fig. 10 featuring an SU(1,1) interferometer diagram, the second OPA is not essential. For realistic quantum systems, we have demonstrated the feasibility of computing the QFI with internal non-Gaussian operations according to the method proposed by Escher et al. [71]. Please see Appendix B for the detailed process. The method is briefly summarized as follows.
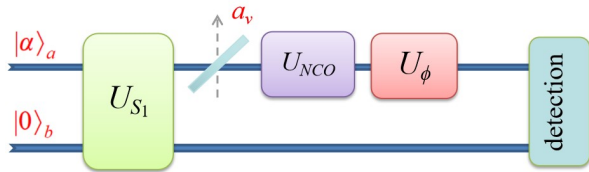

FIG. 10. Schematic diagram of the photon losses on mode a. The losses occurs before the NCO.

For the case of photon losses, we can treat the system as a pure state in an extended space, similar to Eq. (3). Then following Eq. (14), we can obtain the QFI under the pure state, denoted as C_{Q_j}, which is larger or equal to the QFI F_{L_j} for mixed state (our consideration), i.e., $F_{L_j} \leq C_{Q_j}$. C_{Q_j} is the QFI before optimizing over all possible measurements, i.e.,

$$C_{Q_j} = 4\left[\langle\psi|\,\hat{H}_{1_j}\,|\psi\rangle - \left|\langle\psi|\,\hat{H}_{2_j}\,|\psi\rangle\right|^2\right], \qquad (19)$$

where $\hat{H}_{1_j}$ and $\hat{H}_{2_j}$ are defined as

$$\hat{H}_{1_j} = B_j^2 \sum_{l=0}^{\infty} \frac{d}{d\phi}\Pi_l^\dagger\left(\eta,\phi,\lambda\right)U_{p_j}^\dagger U_{p_j}\frac{d}{d\phi}\Pi_l\left(\eta,\phi,\lambda\right) \quad (20)$$

$$\hat{H}_{2_j} = iB_j^2 \sum_{l=0}^{\infty}\left[\frac{d}{d\phi}\Pi_l^\dagger\left(\eta,\phi,\lambda\right)\right]U_{p_j}^\dagger U_{p_j}\Pi_l\left(\eta,\phi,\lambda\right) \quad (21)$$

Here B_j are normalization factors shown in Eq. (B10), and $\Pi_l\left(\eta,\phi,\lambda\right)$ is the phase-dependent Krause operator shown in Eq. (B8), satisfying $\sum\Pi_l^\dagger\left(\eta,\phi,\lambda\right)\Pi_l\left(\eta,\phi,\lambda\right) = 1$, with $\lambda = 0$ and $\lambda = -1$ representing the photon losses before the phase shifter and after the phase shifter, respectively. η is related to the dissipation factor with $\eta = 1$ and $\eta = 0$ being the cases of complete lossless and absorption, respectively. Partiularly, Eqs. (19), (20) and (21) just reduce to these in Ref. [71], when there is no non-Gaussian operations. Following the spirit of Ref. [71], we can further obtain the minimum value of C_{Q_j} by optimizing over λ, corresponding to F_{L_j}, i.e., $F_{L_j} = \min_{\Pi_l(\eta,\phi,\lambda)} C_{Q_j} \leq C_{Q_j}$. See Appendix B about more details.

Next, we further analyze the effects of each parameter on the QFI of the NCO schemes under photon losses by numerical calculation. Fig. 11 is plotted the QIF and QCRB as a function of transmittance η, from which it is observed that the QFI increases with the rising transmittance η, and the NCO can enhance the QFI. This increase can be attributed to the NCO raising the number of photons internally, resulting in higher quantum information, similar to the ideal case. For both non-Gaussian operations, the improved QFI increases with the transmittance η. It is interesting that, over a wide range of about $0 < \eta < 0.85$, the PS-then-PA exhibits a bigger QFI or higher precision than the PA-then-PS. However, as η approaches 1, the PA-then-PS demonstrates a superior QFI/QCRB within the range of about $0.85 < \eta < 1$. This implies that the PS-then-PA presents better performance than PA-then-PS under high dissipation situation.

To explore the underlying reasons for the above case, we further examine the non-classicality of the NCO by the negative volume of Wigner Function (WF) [72]. For simplicity, we only consider the WF of ideal quantum states after non-Gaussian operations. Some details are summarized in Appendix C about the WF. Fig. 12 illustrates the WF in phase space corresponding to two different operations. It is clear that, (i) both non-Gaussian operations can increase the negative volume
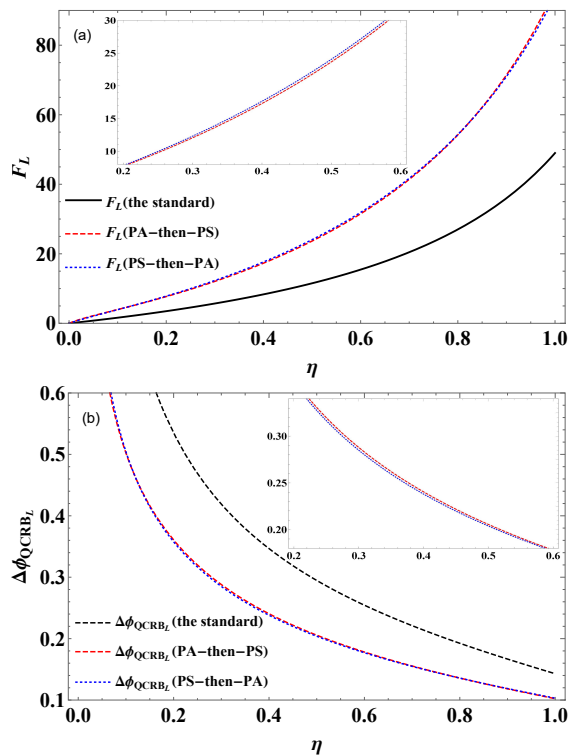
FIG. 11. The F_L and $\Delta\phi_{QCRB_L}$ as functions of transmittance η, with $g=1$ and $\alpha=1$.

FIG. 12. The WF in phase space for quantum states after the NCO with $\alpha=1$. (a)-(d) for the PA-then-PS and (e)-(h) for the PS-then-PA, with several different $g=0.6, 0.8, 1.0, 1.2$ (from left to right).

FIG. 13. (a) The F_L as a function of g, with $\alpha=1$ and $\eta=0.6$. (b) The F_L as a function of α, with $g=1$ and $\eta=0.6$.

of WF, i.e., increase the non-classicality [72]. (ii) For given α and g, the PS-then-PA presents a much bigger negative volume than the PA-then-PS. For example, for $\alpha=1$ and $g=0.6, 0.8, 1.0, 1.2$, the negative volumes are 0.034/0.009, 0.033/0.014, 0.031/0.017, 0.030/0.020 for PS-then-PA/PA-then-PS, respectively. These observations suggest that the non-Gaussian operation increases the non-classicality, and the stronger the nonclassicality of the internal non-Gaussian operation, the more effective it is in suppressing the effect of the internal high noise.

Similar to the ideal case, Fig. 13 illustrates the QFI as a function of g (α) for a given α (g), under the loss case with $\eta=0.6$. Some similar results to Fig. 8 can be obtained, not shown here. Different from the ideal case in Fig. 8, the PS-then-PA scheme performs better than PA-then-PS when g is larger, shown in Fig. 13(a). This case is also true for the QFI with α, shown in Fig. 13(b). These two cases are almost the opposite to the previous ideal situation. The reason may be that the PS-then-PA operation prepares the higher non-classical states, which are more conducive to improve the measurement accuracy, especially in the presence of high photon losses.

V. CONCLUSION

In this paper, we have analyzed the effects of NCO schemes on the phase sensitivity, the QFI and the QCRB
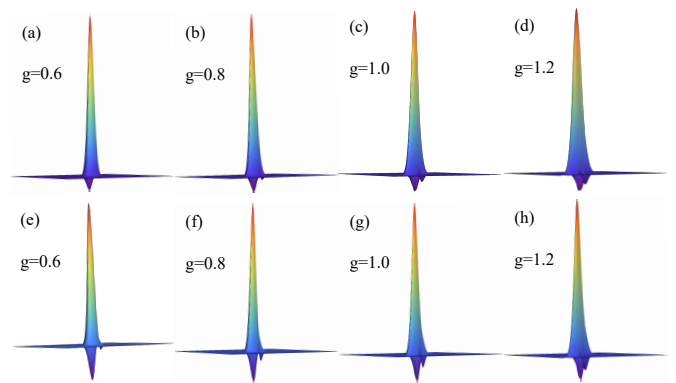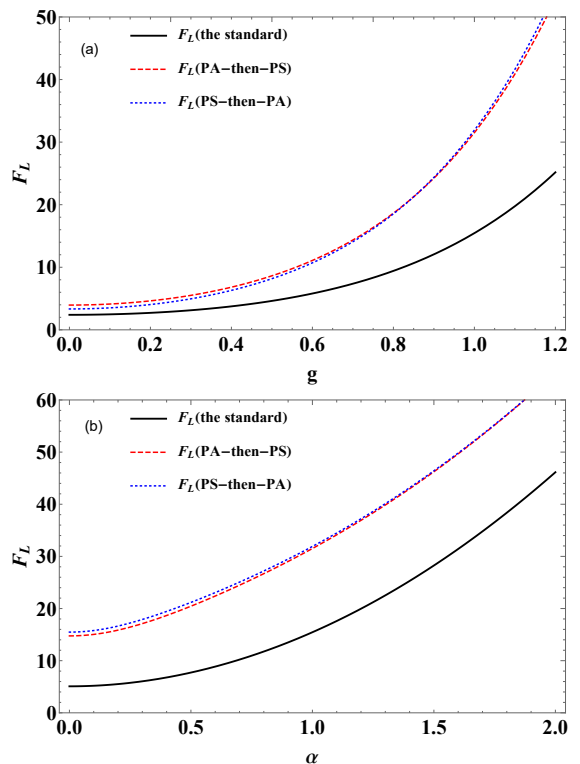
in both ideal and photon losses cases. Additionally, we have investigated the effects of the gain coefficient g of OPA, the coherent state amplitude α and the transmittance T_k of BS on the performance of the system. Through analytical comparison, we have verified that the NCO schemes can improve the measurement accuracy of the SU(1,1) interferometer and enhance the robustness against internal photon losses. The non-Gaussian operations can elevate the total mean photon number of the SU(1,1) interferometer, consequently reinforcing

intramode correlations and quantum entanglement between the two modes.

We further analyze the differences between the two non-Gaussian operations. Concerning the phase sensitivity, the improvement of PS-then-PA is superior in both ideal and photon losses cases. In terms of the QFI and QCRB, in the ideal case, the PA-then-PS is slightly outperforms the PS-then-PA. However, in the photon losses case, the PS-then-PA demonstrates a greater advantage.

In summary, the NCO schemes play a role in overcoming the internal photon losses within SU(1,1) interferometers and in improving the accuracy of quantum measurements. This study highlights the potential of the non-Gaussian operations as valuable tools for improving the performance of quantum metrology and information processing systems. It should be noted that we mainly pay attention to an ideal PS/PA case. Actually, there are some methods to realize these operations. The different experimental parameters will impact the performance, which will be further examined in the near future.

APPENDIX A : THE PHASE SENSITIVITY WITH NCO

In this Appendix, we give the calculation formulas of the phase sensitivity with NCO as follows

$$\Delta\phi_1 = \frac{\sqrt{\langle\Psi^1_{out}|\left(a^\dagger+a\right)^2|\Psi^1_{out}\rangle - \langle\Psi^1_{out}|\left(a^\dagger+a\right)|\Psi^1_{out}\rangle^2}}{|\partial\langle\Psi^1_{out}|\left(a^\dagger+a\right)|\Psi^1_{out}\rangle/\partial\phi|}. \tag{A1}$$

Here, the output state $|\Psi^1_{out}\rangle$ is given by Eq. (3), so the expectations related to the phase sensitivity in PA-then-PS are specifically calculated as follows [53]

$$
\begin{aligned}
&\langle\Psi^1_{out}|\left(a^\dagger+a\right)|\Psi^1_{out}\rangle\\
&=A_1^2[e^{-i\phi}\cosh g\left(P_{3,2,0,0}+4P_{2,1,0,0}+2P_{1,0,0,0}\right)\\
&\quad+\sinh g\left(P_{2,2,0,1}+3P_{1,1,0,1}+P_{0,0,0,1}\right)\\
&\quad+e^{i\phi}\cosh g\left(P_{2,3,0,0}+4P_{1,2,0,0}+2P_{0,1,0,0}\right)\\
&\quad+\sinh g\left(P_{2,2,1,0}+3P_{1,1,1,0}+P_{0,0,1,0}\right)],
\end{aligned}\tag{A2}
$$

and

$$
\begin{aligned}
&\langle\Psi^1_{out}|\left(a^\dagger+a\right)^2|\Psi^1_{out}\rangle\\
&=A_1^2[e^{-2i\phi}\cosh^2 g\left(P_{4,2,0,0}+5P_{3,1,0,0}+3P_{2,0,0,0}\right)\\
&\quad e^{2i\phi}\cosh^2 g\left(P_{2,4,0,0}+5P_{1,3,0,0}+3P_{0,2,0,0}\right)\\
&\quad+2\cosh^2 g\left(P_{3,3,0,0}+5P_{2,2,0,0}+4P_{1,1,0,0}\right)\\
&\quad+2e^{-i\phi}\sinh g\cosh g(P_{3,2,0,1}+4P_{2,1,0,1}\\
&\quad+2P_{1,0,0,1}+P_{3,2,1,0}+4P_{2,1,1,0}+2P_{1,0,1,0})\\
&\quad+2e^{i\phi}\sinh g\cosh g(P_{2,3,1,0}+4P_{1,2,1,0}\\
&\quad+2P_{0,1,1,0}+P_{2,3,0,1}+4P_{1,2,0,1}+2P_{0,1,0,1})\\
&\quad+\sinh^2 g(P_{2,2,0,2}+3P_{1,1,0,2}+P_{0,0,0,2}\\
&\quad+P_{2,2,2,0}+3P_{1,1,2,0}+P_{0,0,2,0}+2P_{2,2,1,1}\\
&\quad+6P_{1,1,1,1}+2P_{0,0,1,1}+2P_{2,2,0,0}\\
&\quad+6P_{1,1,0,0}+2)+A_1^{-2}].
\end{aligned}\tag{A3}
$$

The phase sensitivity with the PS-then-PA can be calculated as

$$\Delta\phi_2 = \frac{\sqrt{\langle\Psi^2_{out}|\left(a^\dagger+a\right)^2|\Psi^2_{out}\rangle - \langle\Psi^2_{out}|\left(a^\dagger+a\right)|\Psi^2_{out}\rangle^2}}{|\partial\langle\Psi^2_{out}|\left(a^\dagger+a\right)|\Psi^2_{out}\rangle/\partial\phi|}, \tag{A4}$$

where the output state $|\Psi^2_{out}\rangle$ is given by Eq. (4), and the expectations associated with the phase sensitivity for the PS-then-PA can similarly be calculated as follows

$$
\begin{aligned}
&\langle\Psi^2_{out}|\left(a^\dagger+a\right)|\Psi^2_{out}\rangle\\
&=A_2^2[e^{-i\phi}\cosh g\left(P_{3,2,0,0}+2P_{2,1,0,0}\right)\\
&\quad+\sinh g\left(P_{2,2,0,1}+P_{1,1,0,1}\right)\\
&\quad+e^{i\phi}\cosh g\left(P_{2,3,0,0}+2P_{1,2,0,0}\right)\\
&\quad+\sinh g\left(P_{2,2,1,0}+P_{1,1,1,0}\right)],
\end{aligned}\tag{A5}
$$

and

$$
\begin{aligned}
&\langle\Psi^2_{out}|\left(a^\dagger+a\right)^2|\Psi^2_{out}\rangle\\
&=A_2^2[e^{-2i\phi}\cosh^2 g\left(P_{4,2,0,0}+3P_{3,1,0,0}\right)\\
&\quad+e^{2i\phi}\cosh^2 g\left(P_{2,4,0,0}+3P_{1,3,0,0}\right)\\
&\quad+2\cosh^2 g\left(P_{3,3,0,0}+3P_{2,2,0,0}+P_{1,1,0,0}\right)\\
&\quad+2e^{-i\phi}\sinh g\cosh g(P_{3,2,1,0}+2P_{2,1,1,0}\\
&\quad+P_{3,2,0,1}+2P_{2,1,0,1})\\
&\quad+2e^{i\phi}\sinh g\cosh g(P_{2,3,0,1}+2P_{1,2,0,1}\\
&\quad+P_{2,3,1,0}+2P_{1,2,1,0})\\
&\quad+\sinh^2 g(P_{2,2,2,0}+P_{1,1,2,0}+P_{2,2,0,2}\\
&\quad+P_{1,1,0,2}+2P_{2,2,1,1}+2P_{1,1,1,1}\\
&\quad+2P_{2,2,0,0}+2P_{1,1,0,0})+A_2^{-2}].
\end{aligned}\tag{A6}
$$

APPENDIX B : THE QFI WITH PHOTON LOSSES

Here, we further examine the QFI with photon losses for the system as shown in Fig. 10. After the first OPA

U_{S_1}, the photon losses, the non-Gaussian operation U_{P_j} ($j = 1$ or 2), and before the detection, the output state in an expanded space can be given by

$$\left| \Psi_{E_j} \right\rangle = B_j U_\phi U_{p_j} U_B \left| 0 \right\rangle_{a_v} \left| \psi \right\rangle, \qquad (B1)$$

a form of pure state, where $\left| \psi \right\rangle = U_{S_1} \left| \alpha \right\rangle_a \left| 0 \right\rangle_b$, and B_j is the normalized factor, determined by $\text{Tr} \left| \Psi_{E_j} \right\rangle \left\langle \Psi_{E_j} \right| = 1$.

For a pure state system, the QFI can be calculated using Eq. (14), denoted as C_{Q_j}. Substituting Eq. (B1) into Eq. (14) yields

$$C_{Q_j} = 4 \left[\left\langle \psi \right| \hat{H}_{1_j} \left| \psi \right\rangle - \left| \left\langle \psi \right| \hat{H}_{2_j} \left| \psi \right\rangle \right|^2 \right], \qquad (B2)$$

where $\hat{H}_{1_j}$ and $\hat{H}_{2_j}$ are operators, defined as

$$\hat{H}_{1_j} = B_j^2 \,_{a_v}\! \left\langle 0 \right| \frac{dU_B^\dagger U_{p_j}^\dagger U_\phi^\dagger}{d\phi} \frac{dU_\phi U_{p_j} U_B}{d\phi} \left| 0 \right\rangle_{a_v}, \qquad (B3)$$

$$\hat{H}_{2_j} = i B_j^2 \,_{a_v}\! \left\langle 0 \right| \frac{dU_B^\dagger U_{p_j}^\dagger U_\phi^\dagger}{d\phi} U_\phi U_{p_j} U_B \left| 0 \right\rangle_{a_v}. \qquad (B4)$$

Noticing $\left[U_\phi, U_{p_j} \right] = 0$, i.e., U_ϕ and U_{p_j} are commutative, and inserting the completeness relation of number state $\sum \left| l \right\rangle_{a_v, a_v} \left\langle l \right| = 1$, one can obtian

$$\hat{H}_{1_j} = B_j^2 \sum_{l=0}^\infty \,_{a_v}\! \left\langle 0 \right| \frac{dU_B^\dagger U_{p_j}^\dagger U_\phi^\dagger}{d\phi} \left| l \right\rangle_{a_v, a_v} \left\langle l \right| \frac{dU_\phi U_{p_j} U_B}{d\phi} \left| 0 \right\rangle_{a_v}$$

$$= B_j^2 \sum_{l=0}^\infty \frac{d}{d\phi} \,_{a_v}\! \left\langle 0 \right| U_B^\dagger U_\phi^\dagger \left| l \right\rangle_{a_v} U_{p_j}^\dagger U_{p_j} \frac{d}{d\phi} \,_{a_v}\! \left\langle l \right| U_\phi U_B \left| 0 \right\rangle_{a_v}$$

$$= B_j^2 \sum_{l=0}^\infty \frac{d}{d\phi} \Pi_l^\dagger (\eta, \phi) U_{p_j}^\dagger U_{p_j} \frac{d}{d\phi} \Pi_l (\eta, \phi), \qquad (B5)$$

and

$$\hat{H}_{2_j} = i B_j^2 \sum_{l=0}^\infty \,_{a_v}\! \left\langle 0 \right| \frac{dU_B^\dagger U_{p_j}^\dagger U_\phi^\dagger}{d\phi} \left| l \right\rangle_{a_v, a_v} \left\langle l \right| U_\phi U_{p_j} U_B \left| 0 \right\rangle_{a_v}$$

$$= i B_j^2 \sum_{l=0}^\infty \left[\frac{d}{d\phi} \Pi_l^\dagger (\eta, \phi) \right] U_{p_j}^\dagger U_{p_j} \Pi_l (\eta, \phi), \qquad (B6)$$

where $\Pi_l^\dagger (\eta, \phi) = \left[\Pi_l (\eta, \phi) \right]^\dagger$ and

$$\Pi_l (\eta, \phi) = \,_{a_v}\! \left\langle l \right| U_\phi U_B \left| 0 \right\rangle_{a_v}$$

$$= \sqrt{\frac{(1-\eta)^l}{l!}} e^{i\phi n} \eta^{\frac{n}{2}} a^l. \qquad (B7)$$

Here, $\Pi_l (\eta, \phi)$ is actually the Kraus operator, describing the photon-losses, and satisfying $\sum \Pi_l^\dagger (\eta, \phi) \Pi_l (\eta, \phi) = 1$, and $n = a^\dagger a$ is the number operator. η is related to the dissipation factor with $\eta = 1$ and $\eta = 0$ being the cases of complete lossless and absorption, respectively.

For a pure state in extended space, the quantum Fisher information C_{Q_j} about the parameter ϕ, is larger or equal to the quantum Fisher information F_{L_j} for mixed state, i.e., $F_{L_j} \leq C_{Q_j}$. C_{Q_j} is the quantum expression for the Fisher in formation before optimizing over all possible measurements. Following the spirit of Ref. [71], i.e., in an interferometer with photon losses in one arm, a possible set of Kraus operators describing the process is

$$\Pi_l (\eta, \phi, \lambda) = \sqrt{\frac{(1-\eta)^l}{l!}} e^{i\phi(n - \lambda l)} \eta^{\frac{n}{2}} a^l, \qquad (B8)$$

also satisfying $\sum \Pi_l^\dagger (\eta, \phi, \lambda) \Pi_l (\eta, \phi, \lambda) = 1$. Here $\lambda = 0$ and $\lambda = -1$ represent the photon losses before the phase shifter and after the phase shifter, respectively. Thus, one can obtain F_{L_j} by optimizing the parameter λ corresponding all possible measurements, i.e.,

$$F_{L_j} = \min_{\Pi_l (\eta, \phi, \lambda)} C_{Q_j} \leq C_{Q_j}. \qquad (B9)$$

In the paper, we shall use Eqs. (B2), (B8), and (B9) to discuss F_{L_j} under photon losses by minimizing C_{Q_j} over λ.

Next, we further derive the normailzation factor B_j. Using Eq. (B1), it is ready to have

$$B_j^{-2} = \sum_{l=0}^\infty \frac{(1-\eta)^l}{l!} \left\langle \psi \right| a^{\dagger l} \eta^n U_{p_j}^\dagger U_{p_j} a^l \left| \psi \right\rangle. \qquad (B10)$$

To obtain the specific expression of B_j^{-2}, we appeal to the technique of integrating within an ordered product of operators (IWOP) [73], i.e., $\eta^n n^q =: \partial^q / \partial x^q \left\{ e^{(\eta e^x - 1)n} \right\} \big|_{x=0} :$, where $: \cdot :$ indicates the symbol of the normal ordering form, which further leads to the formula

$$\sum_{l=0}^\infty \frac{(1-\eta)^l}{l!} l^p a^{\dagger l} \eta^n n^q a^l$$

$$= \frac{\partial^{q+p}}{\partial x^q \partial y^p} \left[\eta e^x + (1-\eta) e^y \right]^n \big|_{x=y=0}. \qquad (B11)$$

Then we can obtain the specific forms for B_1 and B_2, i.e.,

$$B_1 = \left[1 + \left(3\eta - \eta^2 \right) \left\langle \psi \right| n \left| \psi \right\rangle + \eta^2 \left\langle \psi \right| n^2 \left| \psi \right\rangle \right]^{-\frac{1}{2}}, \quad (B12)$$

$$B_2 = \left[\left(\eta - \eta^2 \right) \left\langle \psi \right| n \left| \psi \right\rangle + \eta^2 \left\langle \psi \right| n^2 \left| \psi \right\rangle \right]^{-\frac{1}{2}}, \qquad (B13)$$

where

$$\left\langle \psi \right| n \left| \psi \right\rangle = \alpha^2 \cosh^2 g + \sinh^2 g, \qquad (B14)$$

$$\left\langle \psi \right| n^2 \left| \psi \right\rangle = \alpha^2 \cosh^2 g + \sinh^2 g + \alpha^4 \cosh^4 g$$
$$+ 2 \sinh^4 g + 4\alpha^2 \sinh^2 g \cosh^2 g, \qquad (B15)$$

$$\left\langle \psi \right| n^3 \left| \psi \right\rangle = \alpha^2 \cosh^2 g + \sinh^2 g + 3\alpha^4 \cosh^4 g$$
$$+ 6 \sinh^4 g + 12\alpha^2 \sinh^2 g \cosh^2 g$$
$$+ \alpha^6 \cosh^6 g + 18\alpha^2 \cosh^2 g \sinh^4 g$$
$$+ 6 \sinh^6 g + 9\alpha^4 \cosh^4 g \sinh^2 g, \qquad (B16)$$

and

$$\langle\psi|\,n^4\,|\psi\rangle = \alpha^2\cosh^2 g + \sinh^2 g + 7\alpha^4\cosh^4 g$$
$$+ 14\sinh^4 g + 28\alpha^2\sinh^2 g\cosh^2 g$$
$$+ 36\sinh^6 g + 6\alpha^6\cosh^6 g + 24\sinh^8 g$$
$$+ 108\alpha^2\cosh^2 g\sinh^4 g + \alpha^8\cosh^8 g$$
$$+ 54\alpha^4\cosh^4 g\sinh^2 g + 96\alpha^2\cosh^2 g\sinh^6 g$$
$$+ 72\alpha^4\cosh^4 g\sinh^4 g + 16\alpha^6\cosh^6 g\sinh^2 g. \tag{B17}$$

Here $\langle\cdot\rangle$ is the average under the state $|\psi\rangle$, and $|\psi\rangle = U_{S_1}|\alpha\rangle_a|0\rangle_b$ is the state after the first OPA.

Finally, using Eq. (B11) and Eqs. (B2), (B8), and (B9) to derive C_{Q_j} depending on λ for the PA-then-PS (C_{Q_1}) and for the PS-then-PA (C_{Q_2}), we have

$$C_{Q_1} = 4\{B_1^2(u_1\langle\psi|\,n^4\,|\psi\rangle + u_2\langle\psi|\,n^3\,|\psi\rangle$$
$$+ u_3\langle\psi|\,n^2\,|\psi\rangle + u_4\langle\psi|\,n\,|\psi\rangle)$$
$$- [B_1^2(u_5\langle\psi|\,n^3\,|\psi\rangle + u_6\langle\psi|\,n^2\,|\psi\rangle$$
$$+ u_7\langle\psi|\,n\,|\psi\rangle)]^2\}, \tag{B18}$$

and

$$C_{Q_2} = 4\{B_2^2(u_1\langle\psi|\,n^4\,|\psi\rangle + u_8\langle\psi|\,n^3\,|\psi\rangle$$
$$+ u_9\langle\psi|\,n^2\,|\psi\rangle + u_{10}\langle\psi|\,n\,|\psi\rangle)$$
$$- [B_2^2(u_5\langle\psi|\,n^3\,|\psi\rangle + u_{11}\langle\psi|\,n^2\,|\psi\rangle$$
$$+ u_{12}\langle\psi|\,n\,|\psi\rangle)]^2\}, \tag{B19}$$

where

$$u_1 = \lambda^2\eta^4 - 2\lambda^2\eta^3 + \lambda^2\eta^2 + 2\lambda\eta^4 - 2\lambda\eta^3 + \eta^4, \tag{B20}$$
$$u_2 = -6\lambda^2\eta^4 + 14\lambda^2\eta^3 - 11\lambda^2\eta^2 + 3\lambda^2\eta$$
$$- 12\lambda\eta^4 + 22\lambda\eta^3 - 10\lambda\eta^2 - 6\eta^4 + 8\eta^3, \tag{B21}$$
$$u_3 = 11\lambda^2\eta^4 - 28\lambda^2\eta^3 + 24\lambda^2\eta^2 - 8\lambda^2\eta$$
$$+ \lambda^2 + 22\lambda\eta^4 - 52\lambda\eta^3 + 38\lambda\eta^2$$
$$- 8\lambda\eta + 11\eta^4 - 24\eta^3 + 14\eta^2, \tag{B22}$$
$$u_4 = -6\lambda^2\eta^4 + 16\lambda^2\eta^3 - 14\lambda^2\eta^2 + 4\lambda^2\eta$$
$$- 12\lambda\eta^4 + 32\lambda\eta^3 - 28\lambda\eta^2 + 8\lambda\eta$$
$$- 6\eta^4 + 16\eta^3 - 14\eta^2 + 4\eta, \tag{B23}$$

and

$$u_5 = \lambda\eta^3 - \lambda\eta^2 + \eta^3, \tag{B24}$$
$$u_6 = 6\lambda\eta^2 - 3\lambda\eta - 3\lambda\eta^3 + 5\eta^2 - 3\eta^3, \tag{B25}$$
$$u_7 = 4\eta - \lambda + 4\lambda\eta - 5\lambda\eta^2 + 2\lambda\eta^3 - 5\eta^2 + 2\eta^3, \tag{B26}$$
$$u_8 = -6\lambda^2\eta^4 + 12\lambda^2\eta^3 - 7\lambda^2\eta^2 + \lambda^2\eta$$
$$- 12\lambda\eta^4 + 18\lambda\eta^3 - 6\lambda\eta^2 - 6\eta^4 + 6\eta^3, \tag{B27}$$

as well as

$$u_9 = 11\lambda^2\eta^4 - 22\lambda^2\eta^3 + 13\lambda^2\eta^2 - 2\lambda^2\eta$$
$$+ 22\lambda\eta^4 - 40\lambda\eta^3 + 20\lambda\eta^2$$
$$- 2\lambda\eta + 11\eta^4 - 18\eta^3 + 7\eta^2, \tag{B28}$$
$$u_{10} = -6\lambda^2\eta^4 + 12\lambda^2\eta^3 - 7\lambda^2\eta^2 + \lambda^2\eta$$
$$- 12\lambda\eta^4 + 24\lambda\eta^3 - 14\lambda\eta^2$$
$$+ 2\lambda\eta - 6\eta^4 + 12\eta^3 - 7\eta^2 + \eta, \tag{B29}$$
$$u_{11} = 4\lambda\eta^2 - \lambda\eta - 3\lambda\eta^3 + 3\eta^2 - 3\eta^3, \tag{B30}$$
$$u_{12} = \eta + \lambda\eta - 3\lambda\eta^2 + 2\lambda\eta^3 - 3\eta^2 + 2\eta^3. \tag{B31}$$

Then, we can further optimize λ to get the minimum value of C_{Q_j} using Eq. (19), which corresponding to the F_{L_j}.

APPENDIX C: THE WF WITH NCO

For a two-mode quantum state ρ, its WF under the coherence state representation can be calculated as

$$W_j(z,\gamma) = e^{2(|z|^2+|\gamma|^2)}\int\frac{d^2\beta_a d^2\beta_b}{\pi^4}$$
$$\times\langle-\beta_a,\beta_b|\,\rho\,|\beta_a,\beta_b\rangle$$
$$\times e^{2(z\beta_a^* - z^*\beta_a + \gamma\beta_b^* - \gamma^*\beta_b)}, \tag{C1}$$

where $j = 1$ or 2, and $|\beta_a,\beta_b\rangle = |\beta_a\rangle\otimes|\beta_b\rangle$ are two-mode coherent states. From Eq.(C1), the analytic expression of the WF can be obtained by providing the density operator ρ of the quantum state. Here we only consider the ideal case, i.e., without losses. The quantum state after the NCO is $|\psi_P\rangle = A_j U_{P_j} U_{S_1}|\alpha\rangle_a|0\rangle_b$. Therefore, the density operator ρ can be expressed as

$$\rho = |\psi_P\rangle\langle\psi_P|. \tag{C2}$$

By substituting Eq. (C2) into Eq. (C1), we can obtain the WF after the NCO. Here the specific expressions are not shown for simplicity.

To clearly observe the effect of the gain factor g on the nonclassicality of two different non-Gaussian operations ($aa^\dagger$, $a^\dagger a$), we use the negative volume V_j of the WF to quantitatively describe the non-classicality of the quantum state after the NCO. The calculation formula for the negative volume V_j of the WF is given by

$$V_j = \frac{\int dx_1 dx_2 dy_1 dy_2\,[|W_j(z,\gamma)| - W_j(z,\gamma)]}{2}, \tag{C3}$$

where $z = (x_1 + iy_1)/\sqrt{2}, \gamma = (x_2 + iy_2)/\sqrt{2}$. According to Eq. (C3), the WF negative volume of the state $|\psi_P\rangle$ can be numerically calculated.

[1] G. M. D'Ariano and M. G. A. Paris, Arbitrary precision in multipath interferometry, Phys. Rev. A 55, 2267–2271 (1997).

[2] G. Brida, M. Genovese, and I. R. Berchera, Experimental realization of sub-shot-noise quantum imaging, Nat. Photonics 4, 227–230 (2010).

[3] M. A. Taylor, J. Janousek, V. Daria, J. Knittel, B. Hage, H. A. Bachor, and W. P. Bowen, Biological measurement beyond the quantumlimit, Nat. Photonics 7, 229–233 (2013).

[4] T. Ono, R. Okamoto, and S. Takeuchi, An entanglement-enhanced microscope, Nat. Commun. 4, 2426 (2013).

[5] R. X. Adhikari, Gravitational radiation detection with laser interferometry, Rev. Mod. Phys. 86, 121–151 (2014).

[6] C. Bonato, M. S. Blok, H. T. Dinani, D. W. Berry, M. L. Markham, D. J. Twitchen, and R. Hanson, Optimized quantum sensing with a single electron spin using real-time adaptive measurements, Nat. Nanotechnol. 11, 247–252 (2015).

[7] C. Degen, F. Reinhard, and P. Cappellaro, Quantum sensing, Rev. Mod. Phys. 89, 035002 (2017).

[8] Y. Ma, H. Miao, B. H. Pang, M. Evans, C. Zhao, J. Harms, R. Schnabel, and Y. Chen, Proposal for gravitational-wave detection beyond the standard quantum limit through EPR entanglement, Nat.Phys. 13, 776–780 (2017).

[9] S. Pirandola, B. R. Bardhan, T. Gehring, C. Weedbrook, and S. Lloyd, Advances in photonic quantum sensing, Nat. Photonics 12, 724–733(2018).

[10] C. M. Caves, Quantum-mechanical noise in an interferometer, Phys. Rev. D 23, 1693 (1981).

[11] V. Giovannetti, S. Lloyd, and L. Maccone, Quantum-enhanced measurements: Beating the standard quantum limit, Science 306(5700), 1330–1336 (2004).

[12] V. Giovannetti, S. Lloyd, and L. Maccone, Advances in quantum metrology, Nat. Photonics 5(4), 222–229 (2011).

[13] A. N. Boto, P. Kok, D. S. Abrams, S. L. Braunstein, C. P. Williams, and J. P. Dowling, Quantum interferometric optical lithography: exploiting entanglement to beat the diffraction limit, Phys. Rev. Lett. 85, 2733 (2000).

[14] J. P. Dowling, Quantum optical metrology - the low-down on high-NOON states, Contemp. Phys. 49(2), 125–143(2008).

[15] R. A. Campos, Christopher C. Gerry, and A. Benmoussa, Optical interferometry at the Heisenberg limit with twin Fock states and parity measurements, Phys. Rev. A 68, 023810 (2003).

[16] P. M. Anisimov, G. M. Raterman, A. Chiruvelli, W. N. Plick, S. D. Huver, H. Lee, and J. P. Dowling, Quantum Metrology with Two-Mode Squeezed Vacuum: Parity Detection Beats the Heisenberg Limit, Phys. Rev. Lett. 104, 103602 (2010).

[17] J. Liu, T. Shao, Y. X. Wang, M. M. Zhang, Y. Y. Hu, D. X.Chen, and D. Wei, Enhancement of the phase sensitivity with two-mode squeezed coherent state based on a Mach-Zehnder interferometer, Opt. Express 31, 27735 (2023).

[18] T. Nagata, R. Okamoto, J. L. Obrien, K. Sasaki, and S. Takeuchi, Beating the Standard Quantum Limit with Four-Entangled Photons, Science, 316, 726 (2007).

[19] Z. K. Zhao, H. Zhang, Y. B. Huang, and L. Y. Hu, Phase estimation of a Mach-Zehnder interferometer via the Laguerre excitation squeezed state, Opt. Express 31, 17645(2023).

[20] M. V. Chekhova and Z. Y. Ou, Nonlinear interferometers in quantum optics, Adv. Opt. Photonics 8(1), 104–155(2016).

[21] Z. Y. Ou and X. Li, Quantum su(1,1) interferometers: Basic principles and applications, APL Photonics 5(8),080902 (2020).

[22] B. Yurke, S. L. McCall, and J. R. Klauder, SU(2) and SU(1,1) interferometers, Phys. Rev. A 33(6), 4033–4054(1986).

[23] S. K. Chang, C. P. Wei, H. Zhang, Y. Xia, W. Ye, and L. Y. Hu, Enhanced phase sensitivity with a nonconventional interferometer and nonlinear phase shifter, Phys. Lett. A 384(29), 126755 (2020).

[24] S. K. Chang, W. Ye, H. Zhang, L. Y. Hu, J. H. Huang, and S. Q. Liu, Improvement of phase sensitivity in an SU(1,1) interferometer via a phase shift induced by a Kerr medium, Phys. Rev. A 105(3), 033704 (2022).

[25] C. M. Caves, Reframing SU(1,1) interferometry, Adv. Quantum Technol. 3(11), 1900138 (2020).

[26] D. Scharwald, T. Meier, and P. R. Sharapova, Phase sensitivity of spatially broadband high-gain SU(1,1) interferometers, Phys. Rev. Research 5, 043158 (2023).

[27] F. Hudelist, J. Kong, C. J. Liu, J. T. Jing, Z. Y. Ou, and W. P. Zhang, Quantum metrology with parametric amplifier-based photon correlation interferometers, Nat. Commun. 5(1), 3049 (2014).

[28] J. Jing, C. Liu, Z. Zhou, Z. Y. Ou, and W. Zhang, Realization of a nonlinear interferometer with parametric amplifiers, Appl. Phys. Lett. 99(1), 011110 (2011).

[29] J. Kong, Z. Y. Ou, and W. Zhang, Phase-measurement sensitivity beyond the standard quantum limit in an interferometer consisting of a parametric amplifier and a beam splitter, Phys. Rev. A 87(2), 023825 (2013).

[30] B. Chen, C. Qiu, S. Chen, J. Guo, L. Q. Chen, Z. Y. Ou, and W. Zhang, Atom-light hybrid interferometer, Phys. Rev. Lett. 115(4), 043602 (2015).

[31] B. E. Anderson, P. Gupta, B. L. Schmittberger, T. Horrom, C. Hermann-Avigliano, K. M. Jones, and P. D. Lett, Phase sensing beyond the standard quantum limit with a variation on the SU(1, 1) interferometer, Optica 4(7), 752–756 (2017).

[32] S. S. Szigeti, R. J. Lewis-Swan, and S. A. Haine, Pumped-up SU(1, 1) interferometry, Phys. Rev. Lett. 118(15), 150401 (2017).

[33] G. Frascella, E. E. Mikhailov, N. Takanashi, R. V. Zakharov, O. V. Tikhonova, and M. V. Chekhova, Wide-field SU(1,1) interferometer, Optica 6(9), 1233–1236 (2019).

[34] J. Liu, Y. Wang, M. Zhang, J. Wang, D. Wei, and H. Gao, Ultra-sensitive phase measurement based on an SU(1,1) interferometer employing external resources and substract intensity detection, Opt. Express 28(26), 39443–39452 (2020).

[35] W. Du, J. F. Chen, Z. Y. Ou, and W. Zhang, Quantum dense metrology by an SU(2)-in-SU(1,1) nested interferometer, Appl. Phys. Lett. 117(2), 024003 (2020).

[36] D. Liao, J. Xin, and J. Jing, Nonlinear interferometer based on two-port feedback nondegenerate optical parametric amplification, Opt. Commun. 496, 127137 (2021).

[37] J. D. Zhang, C. You, C. Li, and S. Wang, Phase sensitivity

approaching the quantum Cramér-Rao bound in a modified SU(1,1) interferometer, Phys. Rev. A 103, 032617 (2021).

[38] H. Ma and Y. Liu, Super-resolution localization microscopy: Toward high throughput, high quality, and low cost, APL Photonics 5(6), 080902 (2020).

[39] Y. K. Xu, S. K. Chang, C. J. Liu, L. Y. Hu, and S. Q. Liu, Phase estimation of an SU(1,1) interferometer with a coherent superposition squeezed vacuum in a realistic case, Opt. Express 30, 38178 (2022).

[40] A. M. Marino, N. V. Corzo Trejo, and P. D. Lett, Effect of losses on the performance of an SU(1,1) interferometer, Phys. Rev. A 86(2), 023844 (2012).

[41] Z. Y. Ou, Enhancement of the phase-measurement sensitivity beyond the standard quantum limit by a nonlinear interferometer, Phys. Rev. A 85(2), 023815 (2012).

[42] L. Y. Hu, X. X. Xu, Z. S. Wang, X. F. Xu, Photon-subtracted squeezed thermal state: nonclassicality and decoherence, Phys. Rev. A 82, 043842 (2010).

[43] L. Y. Hu, M. Al-amri, Z. Y. Liao, M. S. Zubairy, Entanglement improvement via a quantum scissor in a realistic environment, Phys. Rev. A 100, 052322 (2019).

[44] L. Y. Hu, Z. Y. Liao, M. S. Zubairy, Continuous-variable entanglement via multiphoton catalysis, Phys. Rev. A 95, 012310 (2017).

[45] H. Zhang, W. Ye, Y. Xia, S. K. Chang, C. P. Wei, and L. Y. Hu, Improvement of the entanglement properties for entangled states using a superposition of number-conserving operations, Laser Phys. Lett. 16, 085204 (2019).

[46] N. Namekata, Y. Takahashi, G. Fujii, D. Fukuda, S. Kurimura, S. Inoue, Non-Gaussian operation based on photon subtraction using a photon-number-resolving detector at a telecommunications wavelength, Nat. Photon. 4, 655–660 (2010).

[47] A. Zavatta, V. Parigi, M. Bellini, Experimental nonclassicality of single-photon-added thermal lightstates. Phys. Rev. A 75, 052106 (2007).

[48] V. Parigi, A. Zavatta, M. Kim, M. Bellini, Probing quantum commutation rules by addition and subtraction of single photons to/from a light field, Science 317, 1890–1893 (2007).

[49] W. Ye, H. Zhong, Q. Liao, D. Huang, L. Y. Hu, Y. Guo, Improvement of self-referenced continuous variable quantum key distribution with quantum photon catalysis, Opt. Express 27, 17186–17198 (2019).

[50] K. Zhang, Y. Lv, Y. Guo, J. Jing, and W.-M. Liu, Enhancing the precision of a phase measurement through phase-sensitive non-Gaussianity, Phys. Rev. A 105, 042607 (2022).

[51] A. Zavatta, V. Parigi, M. S. Kim, H. Jeong, and M. Bellini, Experimental demonstration of the Bosonic commutation relation via superpositions of quantum operations on thermal light fields, Phys. Rev. Lett. 103(14), 140406 (2009).

[52] H. Zhang, W. Ye, C. P. Wei, C. J. Liu, Z. Y. Liao, and L. Y. Hu, Improving phase estimation using number-conserving operations, Phys. Rev. A 103, 052602 (2021).

[53] Y. K. Xu, T. Zhao, Q. Q. Kang, C. J. Liu, L. Y. Hu, and S. Q. Liu, Phase sensitivity of an SU(1,1) interferometer in photon-loss via photon operations, Opt. Express 31(5), 8414 (2023).

[54] C. W. Helstrom, Minimum mean-squared error of esti-

[55] mates in quantum statistics, Phys. Lett. A 25(2), 101 (1967).

[55] C. W. Helstrom, Quantum detection and estimation theory, J. Stat. Phys. 1(2), 231 (1969).

[56] A. Zavatta, S. Viciani, and M. Bellini, Quantum-to-classical transition with single-photon-added coherent states of light, Science 306(5696), 660–662 (2004).

[57] J. Wenger, R. Tualle-Brouri, and P. Grangier, Non-gaussian statistics from individual pulses of squeezed light, Phys. Rev. Lett. 92(15), 153601 (2004).

[58] M. Xiao, L. A. Wu, and H. J. Kimble, Precision measurement beyond the shot-noise limit, Phys. Rev. Lett. 59(3), 278 (1987).

[59] R. Demkowicz-Dobrzański, M. Jarzyna, and J. Kołodyński, Quantum Limits in Optical Interferometry, Prog. Optics 60, 345-435 (2015).

[60] M. Bradshaw, P. K. Lam, and S. M. Assad, Ultimate precision of joint quadrature parameter estimation with a Gaussian probe, Phys. Rev. A 97(1), 012106 (2018).

[61] D. Li, C. H. Yuan, Z. Y. Ou, and W. Zhang, The phase sensitivity of an SU(1,1) interferometer with coherent and squeezed-vacuum light, New J. Phys 16(7), 073020 (2014).

[62] X. Y. Hu, C. P. Wei, Y. F. Yu, and Z. M. Zhang, Enhanced phase sensitivity of an SU(1,1) interferometer with displaced squeezed vacuum light, Front. Phys. 11(3), 114203 (2016).

[63] D. Li, B. T. Gard, Y. Gao, C. H. Yuan, W. Zhang, H. Lee, and J. P. Dowling, Phase sensitivity at the Heisenberg limit in an SU(1,1) interferometer via parity detection, Phys. Rev. A 94(6), 063840 (2016).

[64] S. Ataman, A. Preda, and R. Ionicioiu, Phase sensitivity of a Mach-Zehnder interferometer with single-intensity and difference-intensity detection, Phys. Rev. A 98(4), 043856 (2018).

[65] D. Li, C. H. Yuan, Y. Yao, W. Jiang, M. Li, and W. Zhang, Effects of loss on the phase sensitivity with parity detection in an SU(1,1) interferometer, J. Opt. Soc. Am. B 35(5), 309106 (2018).

[66] L. Y. Hu, M. Al-amri, Z. Y. Liao, and M. S. Zubairy, Continuous-variable quantum key distribution with non-Gaussian operations, Phys. Rev. A 102, 012608 (2020).

[67] Y. Guo, W. Ye, H. Zhong, and Q. Liao, Continuous-variable quantum key distribution with non-Gaussian quantum catalysis, Phys. Rev. A 99, 032327 (2019).

[68] C. M. Caves, Quantum-mechanical noise in an interferometer, Phys. Rev. D 23(8), 1693 (1981).

[69] J. Beltran and A. Luis, Breaking the Heisenberg limit with inefficient detectors, Phys. Rev. A 72(4),045801 (2005).

[70] C. W. Helstrom, Quantum detection and estimation theory (Academic, 1976), 123.

[71] B. M. Escher, R. L. de Matos Filho, and L. Davidovich, General framework for estimating the ultimate precision limit in noisy quantum-enhanced metrology, Nat. Phys. 7(5), 406 (2011).

[72] R. Filip Gaussian quantum adaptation of non-Gaussian states for a lossy channel, Phys. Rev. A 87, 042308 (2013).

[73] H. Y. Fan, H. L. Lu, and Y. Fan, Newton-Leibniz integrationfor ket-bra operators in quantum mechanics and derivation of entangled state representations, Ann. Phys. 321, 480 (2006).